Journal of Hazardous Materials 177 (2010) 458–464

Contents lists available at ScienceDirect

Journal of Hazardous Materials

journal homepage: www.elsevier.com/locate/jhazmat

Photocatalytic activities for hydrogen evolution of new layered compound series $HLaTa_{x/3}Nb_{2-x/3}O_7$/Pt (x = 0, 2, 3, 4, and 6)

Yibin Li, Yunfang Huang, Jihuai Wu*, Miaoling Huang, Jianming Lin

The Key Laboratory for College of Materials Science and Engineering, Huaqiao University of Fujian Higher Education, Institute of Materials Physical Chemistry, Huaqiao University, Quanzhou 362021, China

ARTICLE INFO

Article history:
Received 9 September 2009
Received in revised form 2 November 2009
Accepted 10 December 2009
Available online 21 December 2009

Keywords:
Hydrogen evolution
Photocatalytic activity
Layered compound
Perovskites

ABSTRACT

$HLaTa_{x/3}Nb_{2-x/3}O_7$ were synthesized by successive reactions of conventional solid-state reaction followed by ion exchange reaction. They were characterized by power X-ray diffraction, UV–vis diffusive reflectance and scan electron microscope. The effect of substitution of Ta for Nb in $HLaNb_2O_7$ has been studied on the photocatalytic decomposition of water under UV light irradiation with methanol as electron donor and Pt as promoter catalyst. The x value in $HLaTa_{x/3}Nb_{2-x/3}O_7$ had an important effect on the photocatalytic activity of the catalyst. When x = 2, $HLaTa_{2/3}Nb_{4/3}O_7$/Pt shows a photocatalytic activity of 136 $cm^3\ g^{-1}\ h^{-1}$ hydrogen evolution in rate 10 vol.% methanol aqueous solution under irradiation with wavelength more than 290 nm from a 100-W mercury lamp.

1. Introduction

Photocatalytic reactions of semiconductors, such as splitting of water and reduction of carbon dioxide, have received special attention because of their possible application for the conversion of solar energy into chemical energy. Since the first photocatalyst titanium dioxide suitable for hydrogen evolution from water splitting was reported several decades ago [1], considerable efforts have been devoted to develop a semiconductor photocatalyst for practical application [2–5].

Ion-exchangeable layered perovskites are composed of alternative stacking of a two-dimensional perovskite slab with different numbers of layers and monovalent cations. There are two different typical structures, the Dion–Jacobson series ($A'[A_{n-1}B_nO_{3n+1}]$) and the Ruddlesden–Popper series ($A'_2[A_{n-2}B_nO_{3n+1}]$) [6,7]. A wide variety of compounds in these structural families include titanates, niobates, and tantalates with the d^0 electronic configuration, which have been used as photocatalysts [8–13]. Representative catalysts reported so far include $K_2Ti_4O_9$ [14], $K_4Nb_6O_{17}$ [15], and $K_2La_2Ti_3O_{10}$ [16], which show potential activities for water splitting. The relatively higher photocatalytic activity of these materials than that of the bulk-type simple oxides such as TiO_2 and ZnO has been ascribed to their peculiar structure such as layered or tunnel structures. One interesting feature of these complex mixed-oxides is that their catalytic activity can be highly improved by partial substitution on A- and/or B-sites, with only small changes in the average structure [17–19]. Another characteristic of these layered perovskite is that these layered materials comprised semiconducting host layers and interlayer alkali cations. Charge separation takes place in the host layers upon ultraviolet irradiation. The generated electrons and holes show high reductive and oxidative reactivity, which is the origin of photocatalytic properties. The interlayer guests are ion-exchangeable with various foreign species. Cationic species such as Ni^{2+} and Pt^{4+} have been introduced into interlayer galleries as precursors of photocatalytically active sites [20–24]. The intercalated guest can promote the charge separation on the oxide particle surface and lead to a great increase in the photocatalytic activity.

To further examine the photocatalytic activity of these compounds, new layered oxides $ALaTa_{x/3}Nb_{2-x/3}O_7$ (A = K, H; x = 0, 2, 3, 4 and 6) were prepared. It was found that the novel compounds show good photocatalytic activities for hydrogen evolution [25,26]. The new layered oxide structure upon photocatalytic activity was discussed in this paper.

2. Experimental

2.1. Sample preparation

$KLaTa_{x/3}Nb_{2-x/3}O_7$ layered compound was prepared by conventional solid-state method as described by Sayama et al. [27]. The stoichiometric mixture of carbonates (K_2CO_3) and metal oxides (La_2O_3, Ta_2O_5, Nb_2O_5, 99.99%) was ground for 1 h. An excess amount of carbonate K_2CO_3 (5 mol%) was added to compensate

* Corresponding author. Tel.: +86 595 22693899; fax: +86 595 22693999.
E-mail address: jhwu@hqu.edu.cn (J. Wu).

0304-3894/$ – see front matter © 2009 Elsevier B.V. All rights reserved.
doi:10.1016/j.jhazmat.2009.12.055

the loss due to the volatilization of alkali component during the calcination. Then the mixture was calcined at 1150 °C for 24 h in air with one intermediate regrinding in 12 h to obtain compound $KLaTa_{x/3}Nb_{2-x/3}O_7$. $HLaTa_{x/3}Nb_{2-x/3}O_7$ was prepared by proton exchange reaction of $KLaTa_{x/3}Nb_{2-x/3}O_7$ in 1 M HCl solution at 40 °C for 96 h with intermediate replacement of the acid in each 24 h. After the reaction, the deposit product was washed with distilled water to remove the excess of the acid and then air-dried. $[Pt(NH_3)_4]^{2+}$ was incorporated into the interlayer of $HLaTa_{x/3}Nb_{2-x/3}O_7$ by stirring $HLaTa_{x/3}Nb_{2-x/3}O_7$ (4 g) in 0.6 mM $[Pt(NH_3)_4]Cl_2$ aqueous solution (1000 ml) at room temperature for 72 h. After being filtered and washed with water, the specimen was dispersed in water and irradiated with UV light from a 450 W high-pressure mercury lamp at room temperature for 5 h in order to deposit Pt particles in the interlayer of $HLaTa_{x/3}Nb_{2-x/3}O_7$.

2.2. Characterization

The crystal structure of sample was identified by powder X-ray diffractometer (XRD, Bruker D8 Advance) with monochromated Cu Kα radiation (40 kV, 30 mA, λ = 0.154 nm). Diffuse reflectance spectra were recorded with a Shimadzu UV–VIS–NIR Recording Spectrophotometer UV-3100. The energy band gap was calculated from the onset of the absorption edge of sample in absorption spectrum. The micromorphology of the sample was observed by a SEM (Hitachi S-3500N). The BET surface area was determined by measuring N_2 adsorption isotherm using a Quantachrome instruments Nove4200E Surface area and pore size analyzer after drying at 100 °C for 4 h. The element contents were determined by atomic emission spectroscopy (Intretid xsp radil ict-aes). The chemical compositions of sample were analyzed by Oxford Inca EDX measurements.

2.3. Photocatalytic reaction

Photocatalytic reactions were carried out in a Pyrex reactor of 500 ml capacity attached to an inner radiation type 100 W high-pressure mercury arc lamp. Fig. 1 shows the experimental apparatus used for photocatalytic hydrogen evolution reaction. The reaction system was deaerated by sparging nitrogen for 2 h prior to irradiation. The temperature of the inner cell was controlled via thermostated water flowing through a jacket between the mercury lamp and the reaction chamber. The inner cell was constructed of Pyrex glass, which served to filter out the UV emissions of the mercury arc with wavelengths less than 290 nm. The photocatalytic activities of the samples were evaluated by measuring the volume of the hydrogen gas evolved, using a gas burette, when 1.0 g catalyst sample was dispersed in 500 ml of 10 vol.% methanol solution at 60 °C. Prior to the reaction, the mixture was deaerated by evacuation and then flushed with N_2 (20 kPa) repeatedly to remove O_2 and CO_2 dissolving in water. Before irradiation, it was confirmed that no reaction occurred in the dark. The evolved gas was analyzed by gas chromatography (Shanghai, 102G, molecular sieve 5A column and Ar carrier).

3. Results and discussion

3.1. Morphology and structure

The micromorphology of the samples was observed by a scanning electron microscopy, shown in Fig. 2. All $KLaTa_{x/3}Nb_{2-x/3}O_7$ (x = 0, 2, 3, 4 and 6) samples show well-crystalline and plate-like layered structure, the size of the synthesized $KLaTa_{x/3}Nb_{2-x/3}O_7$ (x = 0, 2, 3, 4 and 6) are about μm order of magnitude.

Fig. 3 shows the powder X-ray diffraction patterns of $KLaTa_{x/3}Nb_{2-x/3}O_7$ series.

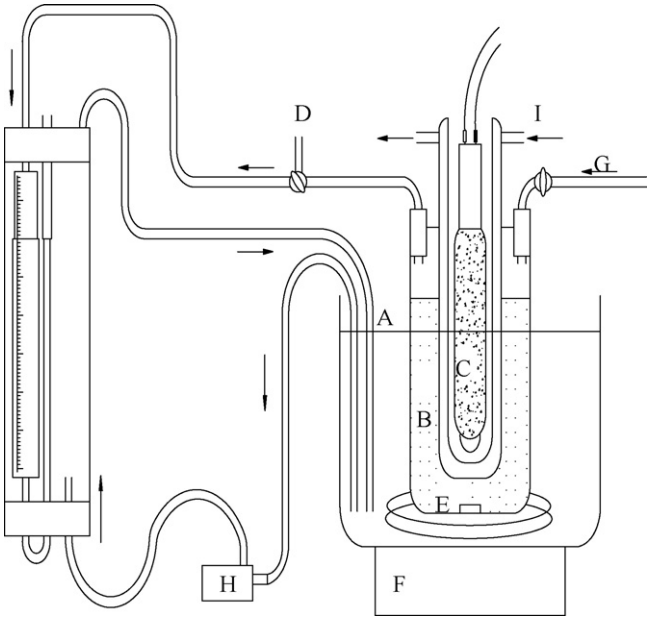

Fig. 1. Schematic illustration of the reaction apparatus used for hydrogen evolution under visible-light irradiation: (A) Pyrex reactor (500 cm^3); (B) pyrex jacket; (C) 100 W high-pressure mercury lamp; (D) three-waycock; (E) magnetic stirrer; (F) temperature controller; (G) gas flow; (H) pump; and (I) cooling and filter solution (1 M $NaNO_2$) three-waycock. The reactor chamber was replaced by N_2 gas before light irradiation.

As an anhydrous compound, $KLaNb_2O_7$ is consisted of single phase layered perovskite structure. The X-ray diffraction patterns are indexed based on orthorhombic lattice with the Cmmm space group by using the JCPDS PDF-2 database (PDF#81-1191) [28–30]. The XRD patterns of the prepared $KLaNb_2O_7$ catalysts are consistent with that of the corresponding compound $KLaNb_2O_7$ in the JCPDS PDF-2 database (PDF#81-1191). The XRD patterns of $KLaTa_{x/3}Nb_{2-x/3}O_7$ ($0 \le x \le 6$) are similar to that of $KLaNb_2O_7$. Therefore, it can be presumed that ($0 < x < 6$) has a same structural model shown in Fig. 4. It is constructed by alternate stacking of triple corner-shared $Ta(Nb)O_6$ octahedra (perovskite slab), La atoms locate at the corner of the octahedra and monoatomic layers of K along the c-axis. Each K ion is coordinated by eight oxygens of $Ta(Nb)O_6$ octahedra in the two adjacent perovskite slabs [31]. Structure refinement of the XRD patterns of $KLaTa_{x/3}Nb_{2-x/3}O_7$ (x = 2, 3, 4, and 6) were performed by assuming the same structural model as that of the niobium compound using the Rietveld method [32].

XRD patterns of $HLaTa_{x/3}Nb_{2-x/3}O_7$ (x = 0, 2, 3, 4 and 6) are shown in Fig. 5. As can be judged from the figure, the positions of diffraction peaks for $HLaTa_{x/3}Nb_{2-x/3}O_7$ ($0 \le x \le 6$) are similar, indicating that $HLaTa_{x/3}Nb_{2-x/3}O_7$ ($0 \le x \le 6$) have similar structures. The XRD patterns of $HLaTa_{x/3}Nb_{2-x/3}O_7$ ($0 \le x \le 6$) prepared are consistent with that of the corresponding compound $HLaNb_2O_7$ in the JCPDS PDF-2 database (PDF#81-1194), which are indexed based on a tetragonal lattice with the P4/m space group known as Dion–Jacobson type [30,31]. The XRD diffraction peaks for $HLaTa_{x/3}Nb_{2-x/3}O_7$ ($0 \le x \le 6$) show a significant shift to higher angle with substitution of Ta for Nb. Since the Ta and Nb have almost same the ionic radii, the c-axis lengths change results from the different interlayer distance. The values of interlayer distances are listed in Table 1. Similar phenomena was also reported by Sayama [27].

Fig. 6 shows the powder X-ray diffraction patterns of $HLaTa_{x/3}Nb_{2-x/3}O_7$/Pt series. The XRD patterns of $HLaTa_{x/3}Nb_{2-x/3}O_7$/Pt are similar with the corresponding compounds without Pt incorporation. The XRD patterns of

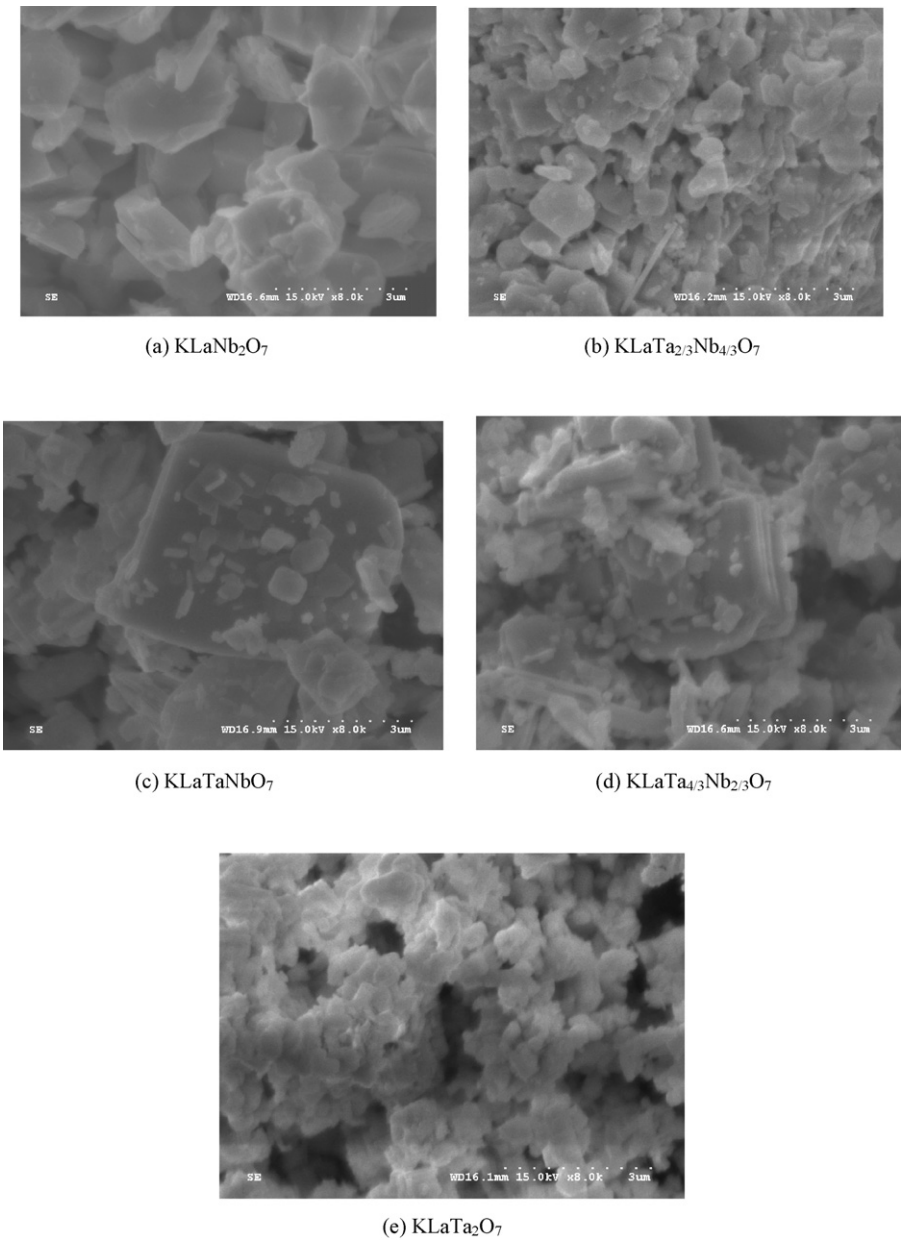

(a) $KLaNb_2O_7$ (b) $KLaTa_{2/3}Nb_{4/3}O_7$

(c) $KLaTaNbO_7$ (d) $KLaTa_{4/3}Nb_{2/3}O_7$

(e) $KLaTa_2O_7$

Fig. 2. SEM photographs of $KLaTa_{x/3}Nb_{2-x/3}O_7$ (x = 0, 2, 3, 4 and 6).

Table 1
Characteristics of $ALaTa_{x/3}Nb_{2-x/3}O_7$/Pt.

x	Sample	Interlayer distance (Å)	Content of Pt (wt%)	Absorption edge (nm)	Band gap (eV)	Surface area ($m^2\ g^{-1}$)
0	$KLaNb_2O_7$	10.94	0	359	3.45	10.46
2	$KLaTa_{2/3}Nb_{4/3}O_7$	10.71	0	343	3.61	11.28
3	$KLaTaNbO_7$	10.91	0	328	3.78	11.17
4	$KLaTa_{4/3}Nb_{2/3}O_7$	10.84	0	321	3.86	10.55
6	$KLaTa_2O_7$	12.82	0	293	4.22	11.82
0	$HLaNb_2O_7$	12.05	0	359	3.45	10.22
2	$HLaTa_{2/3}Nb_{4/3}O_7$	11.95	0	342	3.62	10.63
3	$HLaTaNbO_7$	10.69	0	328	3.78	11.56
4	$HLaTa_{4/3}Nb_{2/3}O_7$	10.56	0	320	3.87	12.42
6	$HLaTa_2O_7$	9.67	0	291	4.25	13.35
0	$HLaNb_2O_7$/Pt	10.77	1.42	362	3.42	10.84
2	$HLaTa_{2/3}Nb_{4/3}O_7$/Pt	10.55	1.03	344	3.60	11.40
3	$HLaTaNbO_7$/Pt	10.56	1.12	333	3.72	11.13
4	$HLaTa_{4/3}Nb_{2/3}O_7$/Pt	10.53	1.18	325	3.81	11.28
6	$HLaTa_2O_7$/Pt	9.79	1.35	316	3.92	12.01

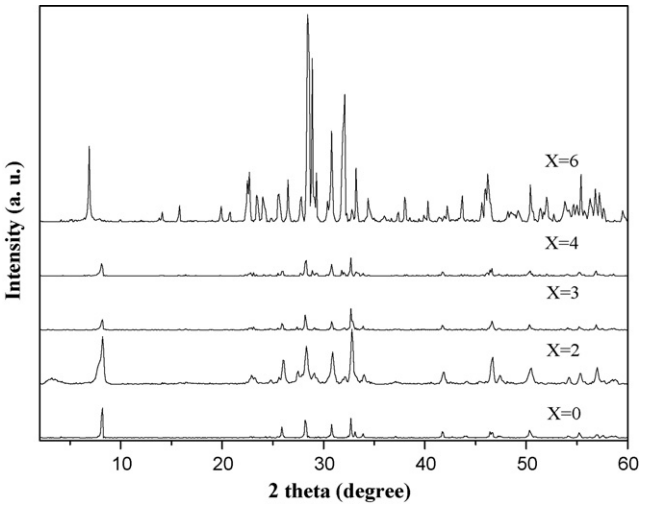

Fig. 3. Powder XRD patterns of $KLaTa_{x/3}Nb_{2-x/3}O_7$ ($x = 0, 2, 3, 4$ and 6).

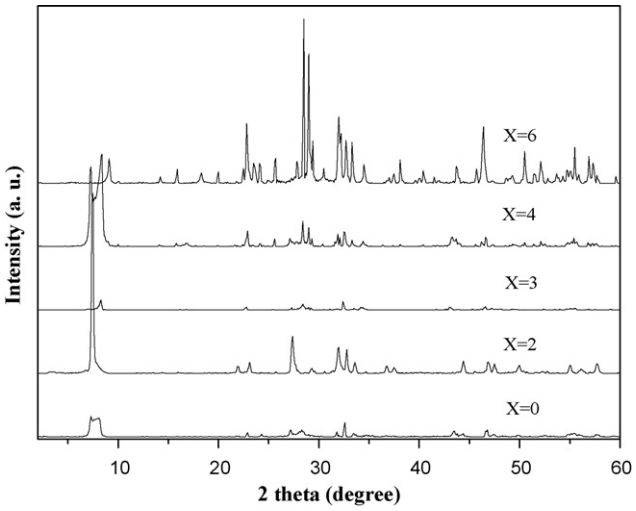

Fig. 5. Powder XRD patterns of $HLaTa_{x/3}Nb_{2-x/3}O_7$ ($x = 0, 2, 3, 4$ and 6).

$HLaTa_{x/3}Nb_{2-x/3}O_7$/Pt ($0 \le x \le 6$) are wondrously consistent with that of the corresponding $HLaNb_2O_7$ compound in the JCPDS PDF-2 database (PDF#81-1194), indicating that ion exchange and Pt incorporation did not cause structure change. No Pt diffraction peaks are found in the $HLaTa_{x/3}Nb_{2-x/3}O_7$/Pt XRD patterns, indicating that Pt is incorporated in the interlayer of $HLaTa_{x/3}Nb_{2-x/3}O_7$. The diffraction peak positions corresponding to the (1 1 0) crystal face of samples are almost the same, but the (0 0 1) crystal face change significantly depending on the species in the interlayer. The results suggest that layered structure of the catalyst still remained after ion exchange and Pt intercalation, although the interlayer distance changes.

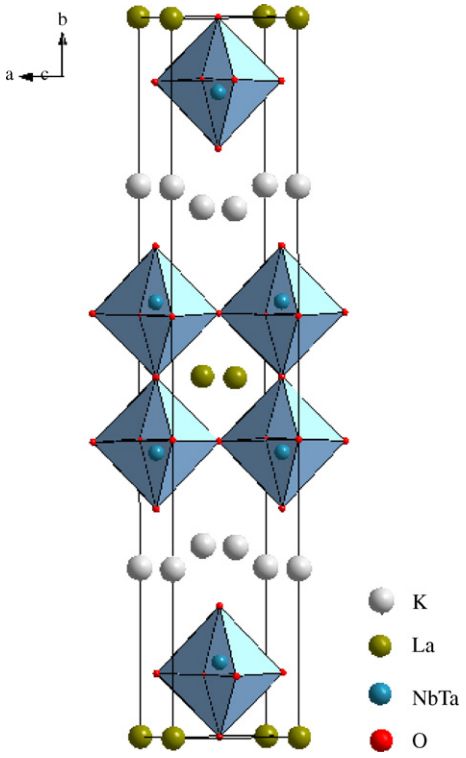

Fig. 4. Structural models of $KLaTa_{x/3}Nb_{2-x/3}O_7$ ($x = 0, 2, 3, 4$ and 6).

3.2. Band gap energy and properties

The compositions of $ALaTa_{x/3}Nb_{2-x/3}O_7$/Pt are examined by EDX measurements, respectively, and the results are closely consistent with the anticipation. The Pt contents are determined by atomic emission spectroscopy (Intretid xsp radil ict-aes) and the special surface area of the samples is measured, respectively. The results are listed in Table 1.

Diffuse reflectance spectra of $ALaTa_{x/3}Nb_{2-x/3}O_7$ (A = K, H; $x = 0$, 2, 3, 4 and 6) are shown in Fig. 7. The absorption edges of $KLaTa_{x/3}Nb_{2-x/3}O_7$ shift to longer wavelength with decreasing the amount of Ta substituted for Nb. The band gaps of tantalum compounds are usually larger than that of niobium compounds, probably because the conduction bands of Ta and Nb compounds originate from 5d orbital of Ta and 4d orbital of Nb, respectively. Moreover, the potential energy of 5d orbital is higher than that of 4d orbital [27]. So that the band gap of the heteropolylanthantantalniobate compounds decreases with decreasing the amount of Ta substituted for Nb in the case of $KLaTa_{x/3}Nb_{2-x/3}O_7$. A shift of absorption edge to longer wavelength is favorable for hydrogen evolution by photocatalytic activity.

The diffuse reflectance spectra of $HLaTa_{x/3}Nb_{2-x/3}O_7$ (Fig. 7b) are almost the same of $KLaTa_{x/3}Nb_{2-x/3}O_7$, which implies that the ion

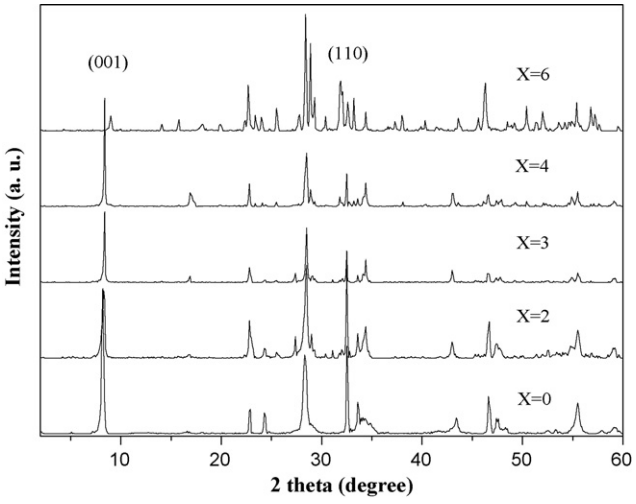

Fig. 6. XRD patterns of $HLaTa_{x/3}Nb_{2-x/3}O_7$/Pt ($x = 0, 2, 3, 4$ and 6).

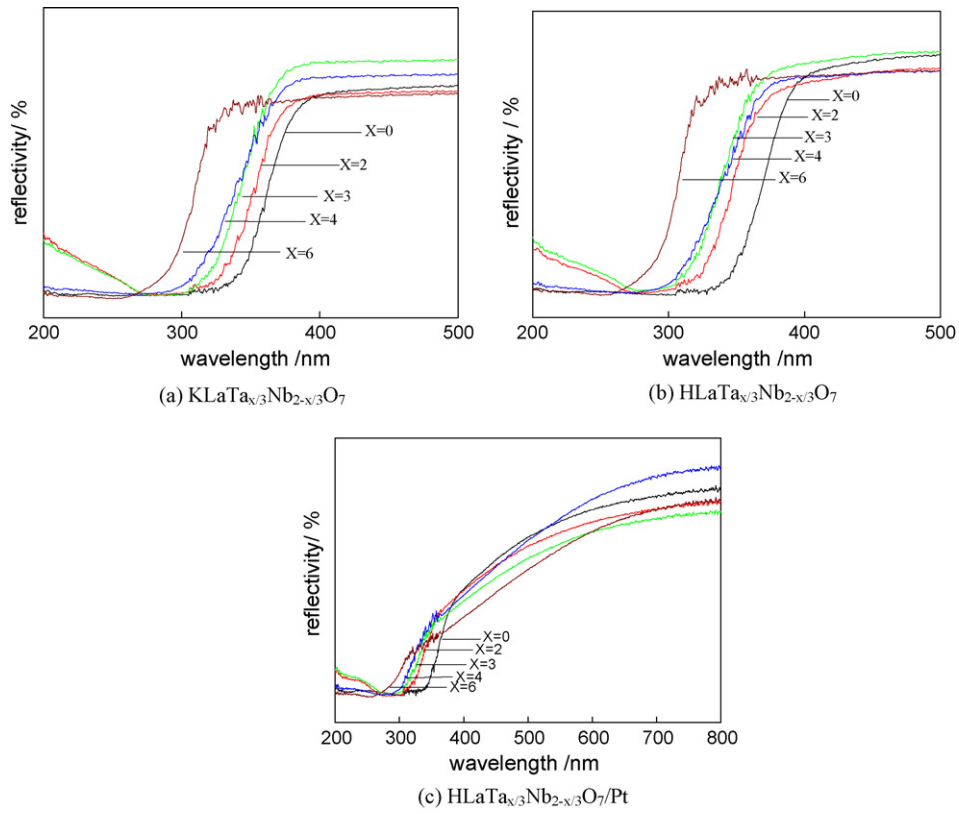

Fig. 7. DRS of ALaTa$_{x/3}$Nb$_{2-x/3}$O$_7$ (A = K, H; x = 0, 2, 3, 4 and 6).

exchange reaction did not change the photoabsorption properties of KLaTa$_{x/3}$Nb$_{2-x/3}$O$_7$.

After incorporation of Pt into the interlayer, the diffuse reflectance spectra of HLaTa$_{x/3}$Nb$_{2-x/3}$O$_7$/Pt (Fig. 7c) show an obvious extension to longer wavelength of absorption band, and HLaTa$_{x/3}$Nb$_{2-x/3}$O$_7$/Pt have absorption band from about 300–800 nm. The addition of Pt could change the scattering properties of the samples and affect the diffuse reflectance spectra.

3.3. Photocatalytic properties

Table 2 and Fig. 8 show the amount of hydrogen gas produced from 500 ml of 10 vol.% methanol solution containing 1 g of dispersed HLaTa$_{x/3}$Nb$_{2-x/3}$O$_7$/Pt at 60 °C for 6 h under irradiation with wavelength more than 290 nm from a 100 W mercury lamp. All samples show high photocatalytic activity. The rate of gas evolved increases in the sequence, TiO$_2$(P-25) « HLaTa$_2$O$_7$/Pt < HLaNb$_2$O$_7$/Pt < HLaTa$_{4/3}$Nb$_{2/3}$O$_7$/Pt < HLaTaNbO$_7$/Pt < TiO$_2$(P-25)/Pt < HLaTa$_{2/3}$Nb$_{4/3}$O$_7$/Pt. Using HLaTa$_{2/3}$Nb$_{4/3}$O$_7$/Pt as catalyst, the photocatalytic H_2 evolution rate reached 136 cm^3 g^{-1} h^{-1} in the presence of methanol as a sacrificial agent for 6 h, which is 45.3 times larger than that of TiO$_2$(P-25) (ca, 3 cm^3 g^{-1} h^{-1}).

Table 2
H_2 gas evolved of HLaTa$_{x/3}$Nb$_{2-x/3}$O$_7$/Pt (x = 0, 2, 3, 4 and 6).

x	Sample	Rate of H_2 gas evolution (cm^3 g^{-1} h)
	TiO$_2$(P-25)	3
	HLaNb$_2$O$_7$	15
	HLaTa$_{2/3}$Nb$_{4/3}$O$_7$	21
	HLaTaNbO$_7$	18
	HLaTa$_{4/3}$Nb$_{2/3}$O$_7$	17
	HLaTa$_2$O$_7$	6
	TiO$_2$(P-25)/Pt	101
0	HLaNb$_2$O$_7$/Pt	34
2	HLaTa$_{2/3}$Nb$_{4/3}$O$_7$/Pt	136
3	HLaTaNbO$_7$/Pt	50
4	HLaTa$_{4/3}$Nb$_{2/3}$O$_7$/Pt	40
6	HLaTa$_2$O$_7$/Pt	17

It is accepted that photocatalyst particles absorb light of energy greater than the band gap to generate electron/hole pairs (Eq. (1)) [33,34]. The electrons are photoinduced to the conduction band (e^-_{CB}) and the holes in the valence band (h^+_{VB}). In the absence of oxygen and presence of sacrificial species such as methanol, the holes generated by the light are trapped by H_2O to yield H^+ and •OH radicals (Eq. (2)), and subsequently the •OH radicals will oxi-

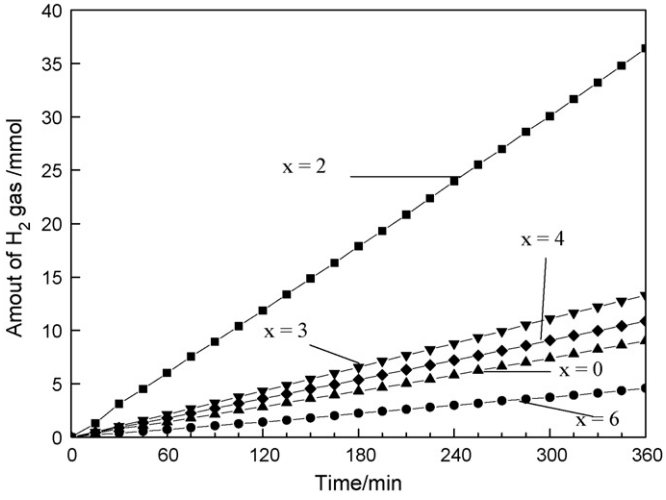

Fig. 8. Time course of H_2 gas evolution from 500 ml of 10 vol.% methanol solution containing 1 g of dispersed HLaTa$_{x/3}$Nb$_{2-x/3}$O$_7$/Pt (x = 0, 2, 3, 4 and 6) at 60 °C for 6 h under irradiation at λ > 290 nm from a 100 W mercury lamp.

dize methanol to HCHO, etc., while electrons in the conduction band of the particle will simultaneously reduce water or protons in the solution to form gaseous H_2 as shown by Eqs. (2)–(5). These reactions proceed competitively with the recombination of the photoinduced electrons and holes.

On the basis of the above results, possible photoreactions on the photocatalysts were proposed as

$$\mathrm{Cat.}\upsilon \xrightarrow{h\nu} \mathrm{Cat.}\ (h^+_{VB} + e^-_{CB}) \quad (1)$$

$$h^+_{VB} + H_2O \rightarrow \cdot OH + H^+ \quad (2)$$

$$CH_3OH + \cdot OH \rightarrow \cdot CH_2OH + H_2O \quad (3)$$

$$\cdot CH_2OH \rightarrow \cdot HCHO + H^+ + e^-_{CB} \quad (4)$$

$$2H_2O + 2e^-_{CB} \rightarrow H_2 + 2OH^- \quad (5)$$

The overall reaction is

$$CH_3OH \xrightarrow{h\nu} HCHO + H_2 \quad (6)$$

In the case of $HLaTa_2O_7$/Pt < $HLaNb_2O_7$/Pt, the difference between the activities of the tantalate and the niobate is likely due to the differences in their band structures. As above discussion, the energy levels of the tops of valence bands of $HLaNbO_7$ and $HLaTaO_7$ are almost the same (2.9 V versus NHE) because their valence bands are formed by p states of oxygen. Based on this understanding, it is thought that tantalate have more negative conduction band energy levels than that niobate does because the former has larger band gap energies than those of the latter [35,36]. From the UV diffuse reflectance spectrum shown in Fig. 7c, the absorption threshold of $HLaNb_2O_7$ is lower than that of $HLaTa_2O_7$ and the band gap of $HLaTa_2O_7$/Pt is estimated to be about 3.92 eV which is larger than that of $HLaNb_2O_7$ (ca. 3.42 eV). Therefore the amount of photon absorbed by $HLaTa_2O_7$ is less than that by $HLaNb_2O_7$.

For the case of photocatalytic activity: $HLaTa_2O_7$/Pt < $HLaTa_{4/3}Nb_{2/3}O_7$/Pt < $HLaTaNbO_7$/Pt < $HLaTa_{2/3}Nb_{4/3}O_7$/Pt. It can be explained that the absorption edges of diffuse reflectance spectra shift to longer wavelength with decreasing the amount of Ta substituted for Nb and the absorbed photon amount by $HLaTa_{x/3}Nb_{2-x/3}O_7$/Pt increases. When $x = 2$, the $HLaTa_{2/3}Nb_{4/3}O_7$/Pt catalyst shows the best photocatalytic activity.

Comparing with $HLaNb_2O_7$/Pt, the $HLaTa_{x/3}Nb_{2-x/3}O_7$/Pt catalyst shows higher photocatalytic activity. For $HLaNb_2O_7$/Pt, Nb is substituted by Ta in Gaussian distribution. A stable $HLaTa_{x/3}Nb_{2-x/3}O_7$/Pt is formed since the Ta and Nb have almost same radii and valence state. We suggest that with the introducing of Ta substituted for Nb, $HLaTa_{x/3}Nb_{2-x/3}O_7$/Pt found a new stable structure type with similar crystal structure that Ta and Nb take the same position of the structure and Gaussian distribution. Because of the large displacement of the Ta ions, it is reasonable to suspect the corresponding changes in its electronic structure and "electronic related" properties of the $HLaNb_2O_7$. Ta doping of $HLaNb_2O_7$ leads to the appearance of the large photoconductivity at low temperatures. $HLaNb_2O_7$ with freezing of Ta in Nb position enhances photoconductivity at low temperatures, which help the separation of photoelectron and photohole, and improve the photocatalytic activity of $HLaTa_{x/3}Nb_{2-x/3}O_7$/Pt. In this special structure, Nb and Ta can be considered as partial substitution particles to A- and/or B-sites, which can highly improve the catalytic activity of the complex mixed-oxides. When $x = 2$, $HLaTa_{2/3}Nb_{4/3}O_7$/Pt found a stable and special structure which the layers formed by NbO_6 and TaO_6 was very suitable for the separation of photo-generated electron–hole pairs and decrease the chance of recombination. It was beneficial to the harvest of light and enhancement of photocatalytic efficiency.

4. Conclusions

From the results described above, the following conclusions can be drawn:

(1) New layered perovskites, $KLaTa_{x/3}Nb_{2-x/3}O_7$ ($x = 0$, 2, 3, 4 and 6) were synthesized by a conventional solid-state reaction. $HLaTa_{x/3}Nb_{2-x/3}O_7$ were synthesized by ion exchange reaction from the parent potassium compounds, $KLaTa_{x/3}Nb_{2-x/3}O_7$. $HLaTa_{x/3}Nb_{2-x/3}O_7$/Pt were synthesized by the deposition of Pt particles in the interlayer of $HLaTa_{x/3}Nb_{2-x/3}O_7$. The crystal structures were refined from powder X-ray diffraction (XRD) patterns as new members of the Dion–Jacobson-type series.

(2) The band gap energies and photocatalytic activities of $HLaTa_{x/3}Nb_{2-x/3}O_7$/Pt depend on the x value (the ratio of Ta to Nb). The $HLaTa_{x/3}Nb_{2-x/3}O_7$/Pt shows excellent photocatalytic activity for H_2 evolution in the presence of methanol as a sacrificial agent under UV irradiation. The gas production rate increases in the sequence TiO_2(P-25) « $HLaTa_2O_7$/Pt < $HLaNb_2O_7$/Pt < $HLaTa_{4/3}Nb_{2/3}O_7$/Pt < $HLaTaNbO_7$/Pt < $HLaTa_{2/3}Nb_{4/3}O_7$/Pt. Especially, $HLaTa_{2/3}Nb_{4/3}O_7$/Pt shows the best photocatalytic activity. The photocatalytic H_2 evolution rate reaches 136 $cm^3\ g^{-1}\ h^{-1}$, which is 45.3 times larger than that of TiO_2(P-25) (ca, 3 $cm^3\ g^{-1}\ h^{-1}$).

Acknowledgements

We acknowledge the financial support from the National High Technology Research and Development Program of China (No. 2009AA03Z217), the National Natural Science Foundation of China (Nos. 50572030 and 50842027), the Key Scientific Technology Program of Fujian, China (No. 2007HZ0001), the Natural Science Foundation of Fujian Province, (No. 2009J01252), and the Science Foundation of Huaqiao University (No. 08Q2R03 and No. 08BS408).

References

[1] A. Fujishima, K. Honda, Electrochemical photolysis of water at a semiconductor electrode, Nature 238 (1972) 37–38.
[2] H. Kato, A. Kudo, Water Splitting into H_2 and O_2 on alkali tantalate photocatalysts $ATaO_3$ (A = Li, Na, and K), J. Phys. Chem. B 105 (2001) 4285–4292.
[3] Z. Zou, J. Ye, H. Arakawa, Direct splitting of water under visible light irradiation with an oxide semiconductor photocatalyst, Nature 414 (2001) 625–627.
[4] A. Fujishima, T.N. Rao, D.A. Tryk, Titanium dioxide photocatalysis, J. Photochem. Photobio. C 1 (2000) 1–21.
[5] H.G. Kim, D.W. Hwang, J. Kim, Y.G. Kim, J.S. Lee, Highly donor-doped (1 1 0) layered perovskite materials as novel photocatalysts for overall water splitting, Chem. Commun. 21 (1999) 1077–1078.
[6] R.E. Schaak, T.E. Mallouk, Perovskites by design: a toolbox of solid-state reactions, Chem. Mater. 14 (2002) 1455–1471.
[7] J. Gopalakrishnan, V. Bhat, $A_2Ln_2Ti_3O_{10}$ (A = potassium or rubidium; Ln = lanthanum or rare earth): a new series of layered perovskites exhibiting ion exchange, Inorg. Chem. 26 (1987) 4299–4301.
[8] Y. Ebina, N. Sakai, T. Sasaki, Photocatalyst of lamellar aggregates of RuO_x-loaded perovskite nanosheets for overall water splitting, J. Phys. Chem. B 109 (2005) 17212–17216.
[9] Y. Inoue, T. Niiyama, Y. Asai, Y. Sato, Stable photocatalytic activity of $BaTi_4O_9$ combined with ruthenium oxide for decomposition of water, J. Chem. Soc. Chem. Commun. 7 (1992) 579–580.
[10] S. Uchida, Y. Yamamoto, Y. Fujishiro, A. Watanabe, O. Ito, T. Sato, Intercalation of titanium oxide in layered $H_2Ti_4O_9$ and $H_4Nb_6O_{17}$ and photocatalytic water cleavage with $H_2Ti_4O_9$/(TiO_2, Pt) and $H_4Nb_6O_{17}$/(TiO_2, Pt) nanocomposites, J. Chem. Soc. Faraday Trans 93 (1997) 3229–3234.
[11] T. Takata, K. Shinohara, A. Tanaka, M. Hara, J.N. Kondo, K. Domen, A highly active photocatalyst for overall water splitting with a hydrated layered perovskite structure, J. Photochem. Photobiol. 106 (1997) 45–49.
[12] T. Ishihara, H. Nishiguchi, K. Fukamachi, Y. Takita, Effects of acceptor doping to $KTaO_3$ on photocatalytic decomposition of pure H_2O, J. Phys. Chem. B 103 (1999) 1–3.
[13] M. Machida, J.I. Yabunaka, T. Kijima, Synthesis and photocatalytic property of layered perovskite tantalates, $RbLnTa_2O_7$ (Ln = La, Pr, Nd, and Sm), Chem. Mater 12 (2000) 812–817.
[14] J.S. Wang, S. Yin, T. Sato, Characterization of $H_2Ti_4O_9$ with high specific surface area prepared by a delamination/reassembling process, Mater. Sci. Eng. B 126 (2006) 53–58.

[15] M.C. Sarahan, E.C. Carroll, M. Allen, D.S. Larsen, Ni.D. Browning, F.E. Osterloh, $K_4Nb_6O_{17}$-derived photocatalysts for hydrogen evolution from water: nanoscrolls versus nanosheets, J. Solid State Chem. 181 (2008) 1678–1683.
[16] C.T.K. Thaminimulla, T. Takata, M. Hara, J.N. Kondo, K. Domen, Effect of chromium addition for photocatalytic overall water splitting on Ni–$K_2La_2Ti_3O_{10}$, J. Catal. 196 (2000) 362–365.
[17] H. Xu, H.M. Li, C.D. Wu, J.Y. Chu, Y.S. Yan, H.M. Shu, Z. Gu, Preparation, characterization and photocatalytic properties of Cu-loaded BiVO4, J Hazard. Mater. 153 (2008) 877–884.
[18] G. Zhang, J. Zhou, X. Ding, Y. Hu, J. Xie, Characterization and photocatalytic properties of Ni-doped $Sr_{10}Bi_6O_{24-y}$, J. Hazard. Mater. 158 (2008) 287–292.
[19] Y. Huang, J. Li, Y. Wei, Y. Li, J. Lin, J. Wu, Fabrication and photocatalytic property of Pt-intercalated layered perovskite niobates $H_{1-x}LaNb_{2-x}Mo_xO_7$ (x = 0–0.15), J. Hazard. Mater. 166 (2009) 103–108.
[20] H.Y. Lin, Y.F. Chen, Y.W. Chen, Water splitting reaction on NiO/$InVO_4$ under visible light irradiation, Int. J. Hydrogen Energy 32 (2007) 86–92.
[21] T. Chen, Z.C. Feng, G.P. Wu, J.Y. Shi, G.J. Ma, P.L. Ying, C. Li, Mechanistic studies of photocatalytic reaction of methanol for hydrogen on Pt/TiO_2 by in situ Fourier Transform IR and time-resolved IR spectroscopy, J. Phys. Chem. C 111 (2007) 8005–8014.
[22] J. Wu, Y. Cheng, J. Lin, Y. Huang, M. Huang, S. Hao, Fabrication and photocatalytic properties of $HLaNb_2O_7$/(Pt, Fe_2O_3) pillared nanomaterial, J. Phys. Chem. C 111 (2007) 3624–3628.
[23] J. Wu, J. Lin, S. Yin, T. Sato, Synthesis and photocatalytic properties of layered $HNbWO_6$/(Pt, $Cd_{0.8}Zn_{0.2}S$) nanocomposites, J. Mater. Chem. 11 (2001) 3343–3347.
[24] J. Wu, S. Uchida, Y. Fujishiro, S. Yin, T. Sato, Synthesis and photocatalytic properties of $HNbWO_6$/TiO_2 and $HNbWO_6$/Fe_2O_3 nanocomposites, J. Photochem. Photobiol. A: Chem. 128 (1999) 129–133.
[25] D.I. Kondarides, V.M. Daskalaki, A. Patsoura, X.E. Verykios, Hydrogen production by photo-induced reforming of biomass components and derivatives at ambient conditions, Catal. Lett. 122 (2008) 26–32.
[26] A. Kudo, Y. Miseki, Heterogeneous photocatalyst materials for water splitting, Chem. Soc. Rev. 38 (2009) 253–278.
[27] K. Sayama, H. Arakawa, K. Domen, Photocatalytic water splitting on nickel intercalated $A_4Ta_xNb_{6-x}O_{17}$ (A = K, Rb), Catal. Today 28 (1996) 175–182.
[28] M. Sato, J. Abo, T. Jin, M. Ohta, Structure determination of $KLaNb_2O_7$ exhibiting ion exchange ability by X-ray powder diffraction, Solid State Ionics 51 (1992) 85–89.
[29] M. Sato, T. Jin, K. Uematsu, Proton conduction of $MLaNb_2O_7$ (M = K, Na, H) with a layered perovskite structure, J. Solid State Chem. 102 (1993) 557–561.
[30] M. Sato, J. Abo, T. Jin, M. Ohta, Structure and ionic conductivity of $MLaNb_2O_7$ (M = K, Na, Li, H), J. Alloys Compd. 192 (1993) 81–83.
[31] M. Machida, K. Miyazaki, S. Matsushima, M. Arai, Photocatalytic properties of layered perovskite tantalates, $MLnTa_2O_7$ (M = Cs, Rb, Na, and H; Ln = La, Pr, Nd, and Sm), J. Mater. Chem. 13 (2003) 1433–1437.
[32] Z. Zou, J. Ye, H. Arakawa, Optical and structural properties of the $BiTa_{1-x}Nb_xO_4$ ($0 \leq x \leq 1$) compounds, Solid State Commun. 119 (2001) 471–475.
[33] T. Kawai, T. Sakata, Photocatalytic hydrogen production from liquid methanol and water, J. Chem. Soc. Chem. Commun. 15 (1980) 694–695.
[34] H. Gerischer, A. Heller, The role of oxygen in photooxidation of organic molecules on semiconductor particles, J. Phys. Chem. 95 (1991) 5261–5267.
[35] D.E. Scaife, Oxide semiconductors in photoelectrochemical conversion of solar energy, Sol. Energy 25 (1980) 41–54.
[36] S. Ikeda, M. Fubuki, Y.K. Takahara, M. Matsumura, Photocatalytic activity of hydrothermally synthesized tantalate pyrochlores for overall water splitting, Appl. Catal. A 300 (2006) 186–190.